



Novel tubular linear actuator with integrated magnetic bearing

Spasoje Mirić · Johann W. Kolar · Dominik Bortis

Received: 23 January 2022 / Accepted: 17 February 2022 / Published online: 18 March 2022
© The Author(s) 2022

Abstract Linear actuators (LAs) are used for applications that require repetitive linear motion, such as linear pumps and compressors, servo drives in industrial automation, and pick-and-place robots in the pharmaceutical and semiconductor industry. These LAs usually have mechanical ball or slide bearings, which require frequent maintenance due to signs of wear limiting the LAs' usage in high-purity and high-precision processes of the latter applications. Therefore, this paper analyzes a novel LA with integrated magnetic bearings (MBs). It shows how the basic structure of the tubular LA is derived from a conventional rotary actuator. Afterwards, it explains the winding structures for the generation of the drive and bearing forces in detail, focusing on the impact of the linear motion on the bearing winding. Furthermore, two types of windings for the self-bearing LA, *separated* and *combined*, are analyzed and compared. It is shown that a combined winding structure leads to higher efficiency and a more simple drive system and has no disadvantages with respect to the control. Finally, measurement results verify the proper operation of a self-bearing tubular LA prototype with a combined winding structure.

Keywords Tubular linear actuator · Magnetic bearings · Self-bearing · Winding concepts

Neuartiger Linearantrieb mit integriertem Magnetlager

Zusammenfassung Linearantriebe werden z. B. für lineare Pumpen und Kompressoren, Servoantriebe in der Industrieautomation oder Pick-and-Place-Roboter in der Pharma- und Halbleiterindustrie zur Ausführung von sich wiederholenden Linearbewegungen eingesetzt. Diese Linearantriebe verfügen typischerweise über mechanische Kugel- oder Gleitlager, welche aufgrund von Verschleißerscheinungen regelmäßig gewartet werden müssen und deshalb den breiten Einsatz in hochreinen und hochpräzisen Prozessen der letztgenannten Anwendungen verunmöglichen. Um diese Nachteile zu beseitigen, wird in diesem Beitrag ein neuartiger Linearantrieb mit integrierten Magnetlagern vorgestellt. Dabei wird zuerst der grundsätzliche Aufbau des magnetisch gelagerten Linearantriebs von einer konventionellen rotierenden Maschine hergeleitet. Anschließend werden die Wicklungsanordnungen zur Erzeugung der Antriebs- und Lagerkräfte detailliert erläutert, wobei dem Einfluss der linearen Bewegung auf die Lagerwicklung und deren Ansteuerung besondere Aufmerksamkeit geschenkt werden.

In einem weiteren Schritt, wird der Realisierungsaufwand des magnetisch gelagerten Linearmotors mit *separaten* oder *kombinierten* Antriebs- und Lagerwicklungen untersucht. Dabei zeigt sich, dass eine kombinierte Wicklungsanordnung zu einer höheren Effizienz und einem einfacheren Antriebssystem führt und auch hinsichtlich Regelung keine Nachteile mit sich bringt. Schließlich wird an einem aufgebauten Prototyp die korrekte Funktionsweise des magnetisch gelagerten Linearmotors mit kombinierter Wicklungsanordnung durch Messergebnisse bestätigt.

S. Mirić (✉) · J. W. Kolar · D. Bortis
Power Electronic Systems Laboratory, ETH Zurich,
Physikstrasse 3, 8092 Zurich, Switzerland
miric@lem.ee.ethz.ch

Schlüsselwörter Linearantrieb · Magnetische Lagerung · Integriertes Lager · Wicklungskonzepte

1 Introduction

Direct drive linear actuators are used in different application areas, ranging from commercial use such as short stroke motors for refrigeration compressors [1–4] and linear actuators for active vehicle suspension [5–7], to linear generators used for wave energy conversion [8–10] and combustion engine piston energy conversion [11–13]. More importantly, linear actuators are used in high-purity and/or high-precision applications in pharmaceutical and semiconductor manufacturing industry, e.g. in pick-and-place robots [14–17].

An example of a linear actuator is shown in Fig. 1, where from a rotary actuator (RA) a tubular linear actuator (TLA) is derived. A tubular structure of the linear actuator is most common in the mentioned applications, as there is no net attraction force between the mover and the stator iron, the stray fields are minimized, and due to the ring-shaped windings and closed structure of the stator iron core, there are no end windings.

Most linear actuators, especially those employed in industrial high-repetitive applications, require frequent maintenance of their bearings [18], such as oiling for the ball bearings or replacements in case slide bearings are used. In addition, mechanical bearings are not suitable for high-purity applications, due to contamination from small particles generated by

abrasion, nor for high-precision applications, due to thermal expansion. Alternatively, for such high-end applications, either air bearings can be used, but they require an external air supply and cannot be employed in low pressure environments, or magnetic bearings (MBs) are used. A major advantage of the TLA with additional MBs is that the mover and the stator do not touch and therefore no contamination due to mechanical friction occurs. In addition, any thermal expansion in a robotic arm holding the TLA can be actively compensated with the MBs by displacing the mover radially off center, which is not possible with either mechanical or air bearings. However, the TLA with ring-shaped windings shown in Fig. 1 cannot generate these bearing forces, so either an additional MB designed as stand-alone machines must be added at both axial ends of the TLA [3] or the ring-shaped windings of the TLA have to be modified such that the MB can be integrated into the TLA as proposed in [16]. This so-called MALTA (Magnetically Levitated Tubular Actuator) is capable to generate a drive and a bearing force onto the mover with the same stator winding, while requiring the same winding volume as the conventional TLA [19, 20]. This paper explains in detail how such actuator and its winding arrangement are derived. First, the linear drive force generation of a conventional TLA is presented in Sec. 2. Then, in Sec. 3, the generation of radial bearing forces with a separated winding is explained, which is then combined with the linear drive winding in Sec. 4. As a result it is shown that the combined drive and bearing windings lead to a reduction

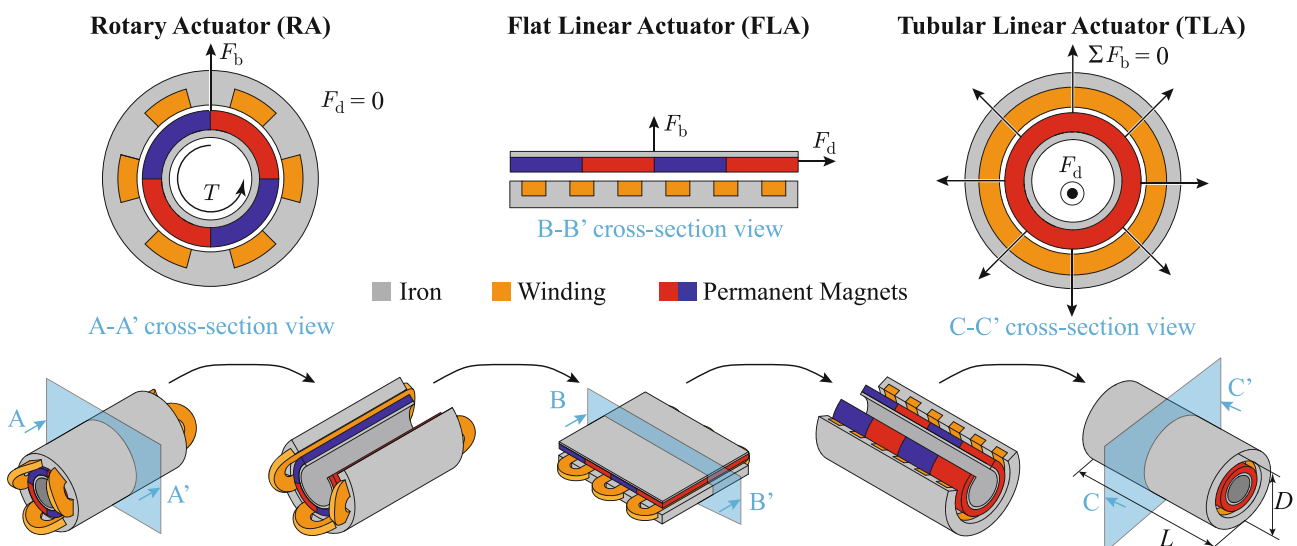


Fig. 1 Illustration of a tubular linear actuator (TLA) derivation from a rotary actuator (RA). Unfolding the RA radially results in a flat linear actuator (FLA), where the drive force F_d of the FLA corresponds to the tangential force in the RA that creates the torque T . The resulting attraction force between the mover and the stator iron, e.g. in case of a magnetically levitated FLA, can be compensated by a bearing force F_b generated by bearing currents in the stator winding. Folding the FLA axially

results in a TLA. The drive force of the TLA stays the same as for the FLA. However, an important advantage is that the net attraction force between the mover and the stator is cancelled out due to the tubular structure of the TLA. The stator winding of the TLA is realized with ring-shaped coils, eliminating any end windings. However, due to the circumferential symmetry of the TLA windings, no bearing forces can be generated

of the stator losses and realization complexity for the overall MALTA system.

Furthermore, it is shown in Sec. 5 that the combined winding arrangement has no negative impact on the complexity of the control structure, i.e., independent controllers for linear motion and the MB control can still be used, but their outputs are then combined before the control signals are applied to the inverter drive.

In Sec. 6, a hardware realization of the MALTA with combined windings and its inverter supply are presented. In addition, measurement results of a position reference step are shown while the bearing controller keeps the mover centered in radial direction. Finally, Sec. 7 concludes the paper.

In the following sections, the force control of a single MALTA module is discussed. Note that two such modules (like depicted in Fig. 8a) are needed for the operation, such that tilting of the mover can be controlled, cf. [16].

2 Drive Force Generation

The drive force generation of the TLA is described with the double-layer three-phase winding arrangement shown in Fig. 2a, since in contrast to the conventionally used single-layer winding, this arrangement can also be used to subsequently explain the bearing force generation. To simplify the analysis, a two-pole machine is assumed where the surface-mounted permanent magnets of the mover indicate the corresponding d- and q-axes in linear direction. The d-axis is aligned with the field axis of the mover's PMs, while the q-axis is electrically phase-shifted by 90°, i.e. by $\pi/2$ rad.

Assuming that in the linear direction only the Lorentz force results in a drive force, but no reluctance force is present, i.e. considering a non-salient pole machine, the fundamental component of the stator flux density must be axially displaced by 90° (i.e. $\theta_1^d = \pi/2$) with respect to the fundamental flux density component generated by the mover's PM in order to produce the Maximum Force Per Ampere (MFPA), as also indicated in Fig. 2a. Consequently, only a stator current in q-direction, i.e. i_q , results in a drive force, which corresponds to the torque-generating current component in a rotary machine. Since the stator current d-component i_d does not generate a drive force, its value is accordingly controlled to zero when the machine is not operated in field weakening mode [19]. In contrast, the amplitude of the q-current \hat{I}_d required to generate the commanded drive force F_d^* , e.g. provided by a position or speed controller, is calculated with the drive force constant K_d as

$$i_d^* = 0 \quad i_q^* = \hat{I}_d = \frac{F_d^*}{K_d} \quad (1)$$

where K_d is either determined by measurement or is analytically calculated (cf. [19]) as

$$K_d = \frac{3\pi}{2\tau_p} \hat{\Psi}, \quad (2)$$

where $\hat{\Psi}$ is the mover flux linkage and τ_p is the PM pole pitch (cf. Fig. 2a). For example, to generate the MFPA for the mover position shown in Fig. 2a, where the q-axis is below phase B, the maximum stator current \hat{I}_d must flow in phase B. Thus, the corresponding currents of the three-phase system are found as $i_A^d = -\hat{I}_d/2$, $i_B^d = \hat{I}_d$ and $i_C^d = -\hat{I}_d/2$, which results in a drive force F_d pointing to the right, as also indicated in Fig. 2a.

In general, however, the required ABC phase currents are determined from the dq-currents with the inverse Park transform Fig. 2b as

$$\begin{aligned} i_A^d &= \hat{I}_d \cos(\theta + \theta_i^d + \gamma_A) \\ i_B^d &= \hat{I}_d \cos(\theta + \theta_i^d + \gamma_B) \\ i_C^d &= \hat{I}_d \cos(\theta + \theta_i^d + \gamma_C), \end{aligned} \quad (3)$$

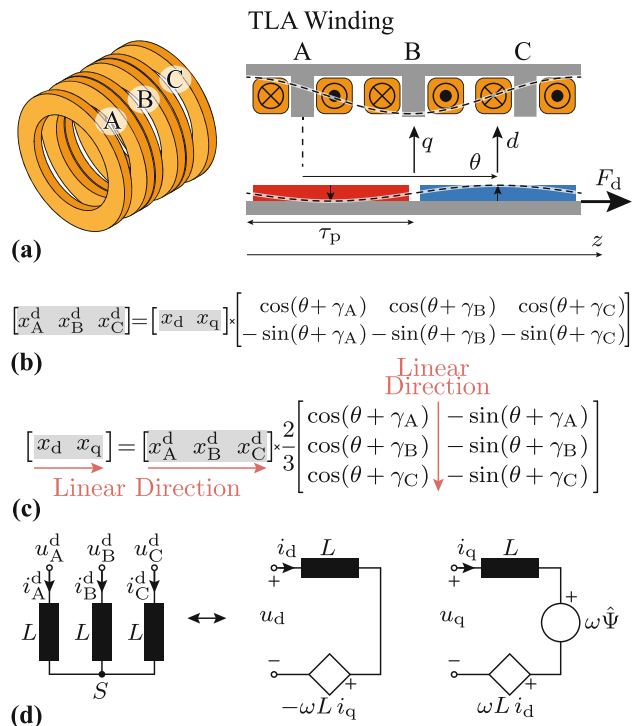


Fig. 2 a TLA double-layer three-phase winding (ABC) and axial cross-section view of the TLA where the dq-frame of the mover is defined. The fundamental flux density components of the mover PM and the drive winding to generate a driving force are also shown. b dq- to ABC-transform (inverse Park transform) and c ABC- to dq-transform (Park transform) used to control the linear drive force of the TLA in the dq-frame. The phase angles are $\gamma_A = 0$, $\gamma_B = -2\pi/3$ and $\gamma_C = 2\pi/3$. d Electrical circuit model of the TLA three-phase linear ABC winding (winding resistance neglected) and its dq-equivalent obtained by the ABC- to dq-transform

where $\theta = \pi z / \tau_p$ is the electrical angle between stator phase A and the d-axis calculated based on the linear mover position z . The electrical angle of the drive current is θ_1^d , which for MFPA equals $\pi/2$, and $\gamma_A = 0$, $\gamma_B = -2\pi/3$, $\gamma_C = 2\pi/3$ are the phase angles that form the three-phase system. Note that (3) can be written in a more compact form

$$i_{\{A,B,C\}} = \hat{I}_d \cos(\theta + \theta_1^d + \gamma_{\{A,B,C\}}), \quad (4)$$

which is used later throughout the paper.

Inversely, to later control the drive currents in the mover-oriented dq-frame, the ABC phase currents must be transformed to dq-currents using the Park transformation given in Fig. 2c. In addition, as will be shown later, to control the dq-currents, the cross-couplings between the dq-axes resulting from the voltages induced by the linear movement and the self-inductance L must be considered (cf. Fig. 2d).

3 Bearing Force Generation

To actively center the mover in the radial direction, it must be possible to apply a radial force, i.e. a bearing force, which can basically be achieved by tangential Lorentz forces or a radial reluctance force [21]. In both cases, this means a redistribution of the air gap flux density in circumferential direction, which is not possible with the already described ring-shaped TLA winding due to its circumferential symmetry. One possibility is to accommodate an additional two-phase bearing winding in the stator of the TLA, which enables active control of the radial position.

As shown in Fig. 3a, the two-phase bearing winding basically consists of two pairs of windings $-xA$ and xA or $-yA$ and yA , which can generate either a bearing force F_x in the x-direction or a bearing force F_y in the y-direction.

For example, for the case shown in Fig. 3a, if a positive bearing current i_x is impressed in the xA and a negative i_x in the $-xA$ winding, a stator flux density is generated in the positive x direction. If it is also assumed that a ring magnet magnetized radially outward is located below the bearing winding, a radial force is generated in the positive x-direction. This can be explained by the fact that due to the superposition of the radial flux density of the mover ring magnet and the x-directed stator field, the total flux density in the air gap is increased on the right side and reduced on the left side, resulting in a stronger attraction of the mover to the right stator tooth due to the reluctance force. Alternatively, each pair of bearing windings can be thought of as two equivalent permanent magnets with north (N) and south (S) poles, with N and S attracting on the right side and N and N repelling on the left. Similarly, a force F_y in the y-direction can be generated with bearing current i_y and $-i_y$ in the winding pair yA and $-yA$. The superposition of the two forces F_x and F_y finally leads to a radial bearing force space

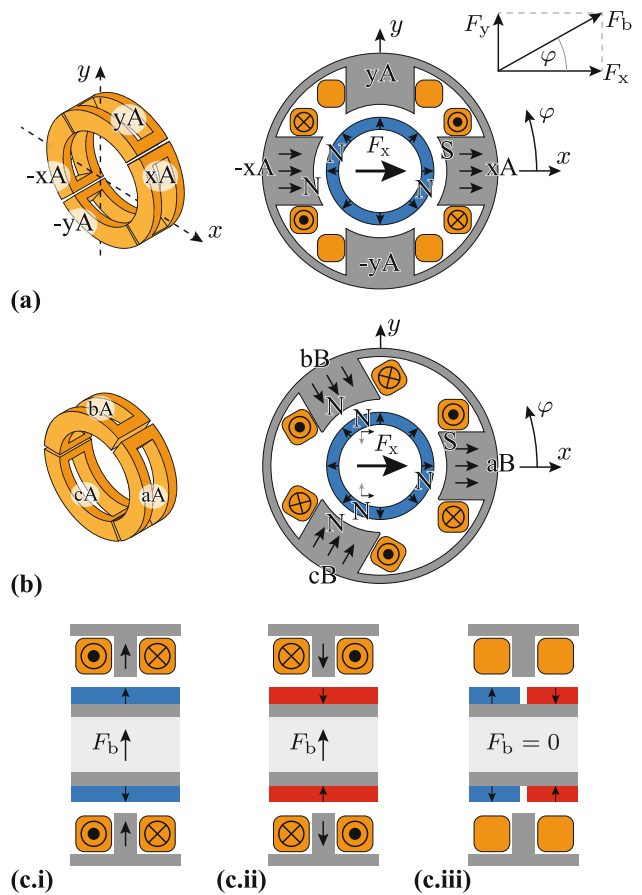


Fig. 3 Possible winding arrangements to generate bearing forces: **a** two-phase xy- and **b** three-phase abc-bearing winding. Three possible mover positions in axial direction facing the bearing winding, where in **c.i** and **c.ii** a MFPA can be generated, but the current direction must reverse to keep the bearing force constant, while in **c.iii** no bearing force can be generated

vector (cf. Fig. 3a) whose length F_b corresponds to the total bearing force and the angle φ determines the direction of the bearing force, i.e.

$$F_b = \sqrt{F_x^2 + F_y^2}, \quad \varphi = \arctan 2(F_x, F_y). \quad (5)$$

In analogy to the drive force, the relationship between either the total bearing force F_b and the total bearing current \hat{I}_b or the individual xy-bearing current components and the required xy-bearing forces, e.g. provided by xy-position controllers, is given by a bearing force constant K_b as

$$i_x^* = \frac{F_x^*}{K_b} = \hat{I}_b \cos(\varphi), \quad i_y^* = \frac{F_y^*}{K_b} = \hat{I}_b \sin(\varphi), \quad (6)$$

where $\hat{I}_b = F_b / K_b$ is the length of the corresponding total bearing current space vector. Instead of using a two-phase xy-bearing winding, a radial bearing current vector can also be generated with a circum-

ferentially distributed three-phase abc-bearing winding, as shown in Fig. 3b. The required instantaneous abc-bearing currents result from the projection of the bearing current space vector onto the phase axes, or is mathematically given as

$$\begin{aligned} i_a &= \hat{I}_b \cos(\varphi + \gamma_a) \\ i_b &= \hat{I}_b \cos(\varphi + \gamma_b) \\ i_c &= \hat{I}_b \cos(\varphi + \gamma_c), \end{aligned} \quad (7)$$

where the rotary phase angles of the three-phase bearing winding are equal to $\gamma_a = 0$, $\gamma_b = -2\pi/3$, $\gamma_c = 2\pi/3$. For completeness, Fig. 3b shows the flux directions and the required three-phase bearing currents, i.e. $i_a = \hat{I}_b$, $i_b = -\hat{I}_b/2$ and $i_c = -\hat{I}_b/2$, to achieve the same positive bearing force F_x as in Fig. 3a with two-phase bearing currents.

Considering now the bearing force generation in the TLA, it must also be taken into account that the direction of the radial magnetization of the mover PM located in the bearing stator changes as a function of the linear z-position of the mover and thus a constant bearing current would lead to different bearing forces depending on the z-position. So, for example, if the direction of radial magnetization of the mover PM located inside the MB reverses, the direction of the bearing current vector must also be reversed to keep the bearing force constant, as it is shown in Fig. 3c.i and c.ii. However, this only applies if the PM mover is axially aligned with the MB stator. Consequently, if the mover is e.g. positioned axially such that two adjacent mover PMs are each half inside the MB stator, no bearing force can be generated because the mover is attracted as much as it is repelled (cf. Fig. 3c.iii).

Thus, in order to always ensure a bearing force for the TLA at any z-position of the mover, multiple pairs of bearing windings must be arranged in the axial direction as shown in Fig. 4a. This can be achieved, for example, with a three-phase ABC-winding in the axial direction, which in the simplest case just covers one pole pair of the mover. For example, to generate a bearing force in the y-direction, the bearing winding pairs -yB with yB and -yC with yC are required in addition to the bearing winding pair -yA and yA, resulting in a 2×3 bearing winding configuration, which indicates the number of circumferential phases times the axial phases.

The currents i_{yA} , i_{yB} and i_{yC} flowing through the axially arranged bearing winding pairs yA, yB and yC must now be selected in such a way that the fundamental components of the flux density distribution generated by the bearing currents and the mover PMs are in phase with each other in the axial direction, i.e. $\theta_i^b = 0$ (cf. cross-section in Fig. 4a). In this case, a maximum bearing force (MFPA) is achieved for a given bearing current amplitude, which in the axial direction of the mover-oriented dq-frame corresponds to a pure d-current component. In contrast, a q-component of the bearing current would

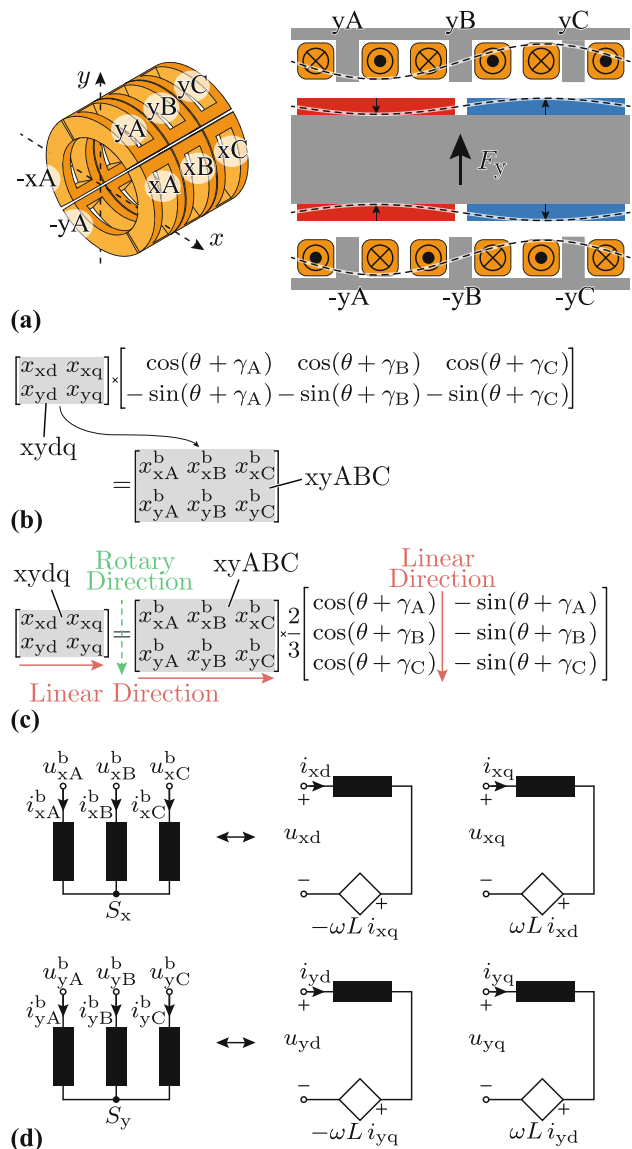


Fig. 4 a Realization of the 2×3 bearing winding (xyABC) and axial cross-section view with indicated fundamental flux density components of the mover PM and the bearing winding to generate bearing forces. b xydq- to xyABC-transform (inverse Park transform) and c xyABC- to xydq-transform (Park transform) used to control the bearing force of the 2×3 winding in the dq-frame. The phase angles are $\gamma_A = 0$, $\gamma_B = -2\pi/3$ and $\gamma_C = 2\pi/3$. d Electrical circuit model of the 2×3 bearing winding and its dq-equivalent

result in a stator field that in the axial direction is 90° phase-shifted with respect to the mover field and thus would not generate any bearing forces. Consequently, the q-components of the xy-bearing currents are controlled to zero, while the d-components are directly derived from the xy-bearing forces e.g. commanded by the radial xy-position controllers as

$$\begin{aligned} i_{xd}^* &= i_x^* = \frac{F_x^*}{K_b} & i_{xq}^* &= 0 \\ i_{yd}^* &= i_y^* = \frac{F_y^*}{K_b} & i_{yq}^* &= 0, \end{aligned} \quad (8)$$

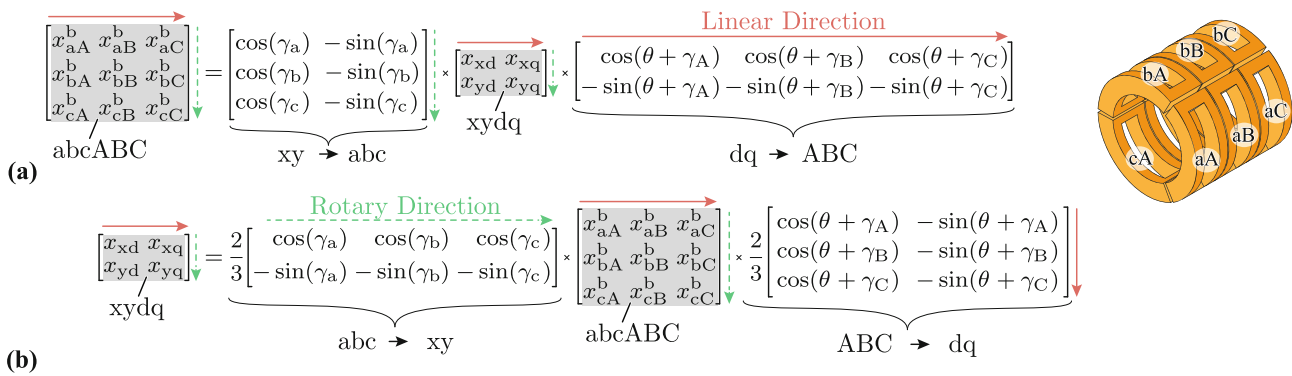


Fig. 5 **a** xydq- to abcABC-transform (inverse Clarke & Park transform) and **b** abcABC- to xydq-transform (Clarke & Park transform) used to control the bearing force of the 3×3 bearing winding (abcABC) in the dq-frame

which actually coincides with (6). Thus, the current components i_{xd}^* or i_{yd}^* only indicate how large the total bearing current must be in the x- or y-direction to generate the commanded bearing force F_x^* and F_y^* .

As mentioned, in a further step, these bearing currents must be distributed to the three axially arranged xy-bearing winding pairs depending on the z-position, which again can either be understood as a projection of a dq-space vector onto the three-phase winding axes in axial direction or is mathematically expressed with the inverse Park transform (cf. Fig. 4b) as

$$\begin{aligned} i_{x\{A,B,C\}}^* &= i_{xd}^* \cdot \cos(\theta + \theta_i^b + \gamma_{\{A,B,C\}}) \\ i_{y\{A,B,C\}}^* &= i_{yd}^* \cdot \cos(\theta + \theta_i^b + \gamma_{\{A,B,C\}}), \end{aligned} \quad (9)$$

where θ_i^b is the electrical angle of the bearing current in linear direction and for MFPA is set to 0° , and $\gamma_{\{A,B,C\}} = \{0, -2\pi/3, 2\pi/3\}$ are the phase angles of the three-phase bearing system in axial direction.

If a three-phase abc-bearing winding is used along the circumference instead of a two-phase xy-winding, i.e. a 3×3 bearing winding, its phase currents given in (7) are also modulated according to the z-position of the mover, which finally leads to the following nine bearing currents

$$\begin{aligned} i_{a\{A,B,C\}}^b &= \hat{I}_b \cos(\varphi + \gamma_a) \cdot \cos(\theta + \theta_i^b + \gamma_{\{A,B,C\}}) \\ i_{b\{A,B,C\}}^b &= \hat{I}_b \cos(\varphi + \gamma_b) \cdot \cos(\theta + \theta_i^b + \gamma_{\{A,B,C\}}) \\ i_{c\{A,B,C\}}^b &= \hat{I}_b \cos(\varphi + \gamma_c) \cdot \cos(\theta + \theta_i^b + \gamma_{\{A,B,C\}}), \end{aligned} \quad (10)$$

where \hat{I}_b and φ can be determined in analogy to (5), but just expressed by the commanded dq-currents i_{xd}^* and i_{yd}^* as $\hat{I}_b = \sqrt{(i_{xd}^*)^2 + (i_{yd}^*)^2}$ and $\varphi = \arctan2(i_{xd}^*, i_{yd}^*)$.

This transformation from the dq- to the three-phase abc-bearing winding is also performed by the inverse Clarke & Park transform given in Fig. 5a). Illustratively speaking, based on (10) the bearing currents and thus the resulting air gap field generating the bearing force changes sinusoidally in both axial and radial directions, while for the drive force the field changes sinusoidally only in the axial direction (cf. (4)). This sinusoidal distribution of the bearing current in both directions also means that in both di-

rections no common-mode (CM) current component is needed to generate any bearing force and therefore e.g. the 3×3 bearing winding can be connected to three independent three-phase windings with three independent star points, where either always the three circumferentially or three axially arranged coils are connected in a star point. Similarly, since the drive currents are changing sinusoidally in axial direction, the three axially arranged ring-shaped phase windings can be connected in a star point.

In analogy to the drive current in Sect. 2, in order to later control the bearing currents in the mover-oriented dq-frame, the xyABC- or abcABC-phase currents must be transformed to dq-currents using the Park transform given in Fig. 4c or the Clarke & Park transform given in Fig. 5b). In addition, Fig. 4d shows the equivalent circuits in the dq-frame including the cross-couplings between the d- and q-axes resulting from the self-inductance L only. There it is assumed that the three axially displaced bearing windings are always connected to a common star point.

4 Separated or Combined Drive and Bearing Windings

Based on the previous considerations, a TLA with MB can be realized, for example, with two electrically but not magnetically *separated winding* systems, i.e. dedicated drive and bearing windings are accommodated in the slots of the same stator. In this case, it is desired that no coupling of forces can occur between the winding systems, which means that the drive winding system generates only drive forces and the bearing winding system only bearing forces. If this is ensured, the drive and bearing control can also be considered separately decoupled from each other, i.e. for the control of the drive force or the z-position only the currents $i_{\{A,B,C\}}^d$ in the drive winding and for the control of the bearing force or xy-positions only the currents in the bearing winding $i_{\{x,y\}\{A,B,C\}}^b$ or $i_{\{a,b,c\}\{A,B,C\}}^b$ have to be considered. Otherwise, the bearing currents would also have to be taken into account in the drive control or vice versa.

As already mentioned, the ring-shaped three-phase drive winding can only generate a linear force, but no bearing force. For the bearing winding, however, it must be investigated in more detail whether a drive force can be generated, since, as already described, there are various possibilities for realizing the bearing winding. In a first case, the bearing winding can be realized e.g. with a 2×3 winding arrangement. As shown in Fig. 6a, the radially opposite x- or y-windings are first connected antiseri- ally and then axially in a star configuration. This winding configuration ensures that no common-mode (CM) bearing current can flow in either the axial or circumferential direction, thus preventing a driving force. Such a driving force is actually only possible if the circumferentially arranged bearing windings generate a CM bearing current component, i.e. a current flowing in the same direction in all these windings, as would be the case with the ring-shaped drive winding. In addition, this winding configuration also minimizes the complexity of the power electronics to a total of 9 half-bridges, where in total only 6 phase currents need to be measured for drive and bearing control.

Alternatively, as shown in Fig. 6b, the separated bearing winding can also be implemented with a 3×3 winding arrangement. As mentioned above, based on (10), no CM current is required in either the axial or circumferential direction to generate the bearing force, so the 9 bearing coils may be connected in star in both directions. If the bearing windings are connected in star in the axial direction, however, a CM bearing component can basically flow in the circumferential direction, resulting in an undesired drive force. Due to the abc/dq-transformation of the abcABC- into the xydq-bearing currents (cf. Fig. 5b), this CM component is lost and is therefore not visible for the bearing control and thus cannot be compensated (the transformation would have to provide the additional information of the zero-sequence component, i.e. the dq0-transform, and an additional controller would have to control this quantity to zero). Consequently, to prevent a CM component in the circumferential direction, the bearing windings arranged in the circumferential direction must be connected in star. Thus, in principle, a CM component in the axial direction is possible, but this results neither in a driving force nor in a bearing force and only causes additional conduction losses (to prevent this zero-sequence component, the dq0-transform and an additional controller are again required). The appropriate circuit is shown in Fig. 6b, where a total of 12 stator coils and half-bridges, and 8 current measurements are required.

The major disadvantages of the *separated windings* are the high implementation effort of the stator and the fact that the two winding systems have to share the stator slots. In this case, the available copper cross-section of the individual winding systems is defined by the separation of the conductors and the additional

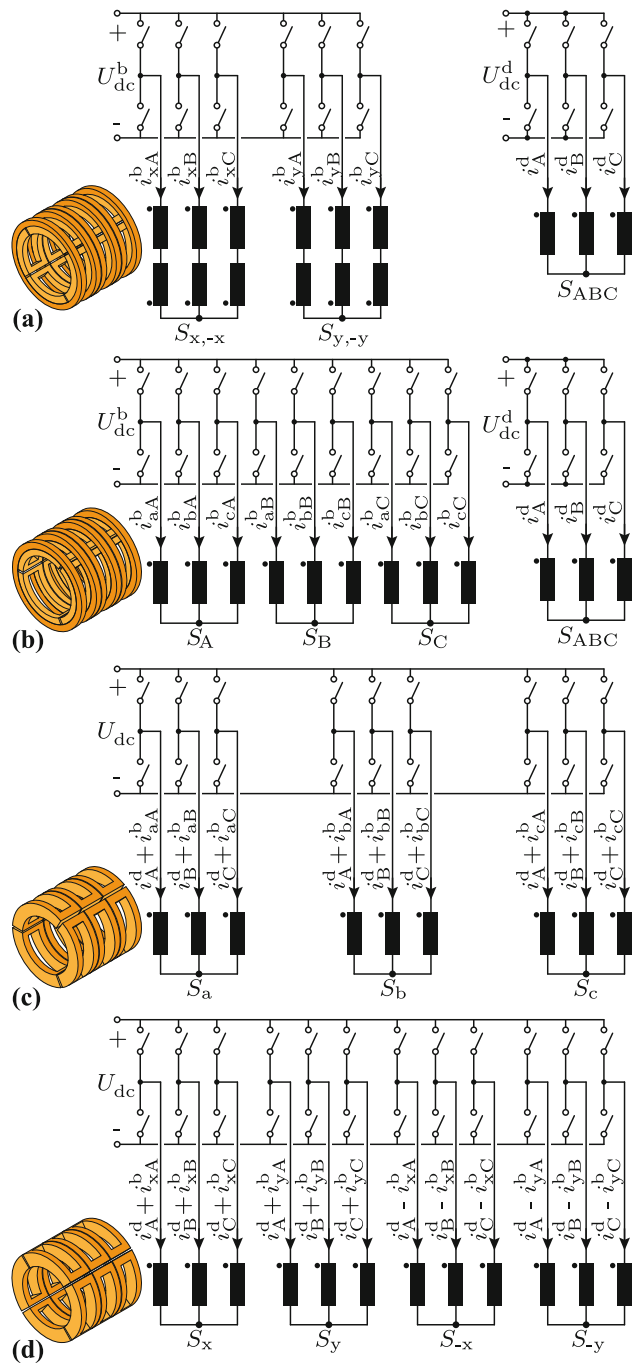


Fig. 6 Possible MALTA winding configuration for *separate* drive and bearing force generation, i.e. a ring-shaped drive winding together with either **a** a 2×3 bearing winding having an antiseri-connection of the xy-windings and axial star point or **b** a 3×3 bearing winding having a star point connection in circumferential direction; and for *combined* drive and bearing force generation, i.e. **c** a 3×3 or **d** a 2×3 drive and bearing, both having axially arranged star points, cf. [22]

insulation reduces the fill factor. Most important, the individual copper cross-sections are not optimally utilized in most operating ranges, since the distribution of the conductor cross-sections depends on the operating point and, especially the required bearing force is determined by the installation and the additional

weight of the load. Optimal design of the actuator is therefore difficult and in most cases is done for the worst case. The separated winding arrangement thus leads to increased conduction losses – not only because of the lower fill factor, but also because of the physical separation of the currents.

A physical separation of drive and bearing currents is basically not necessary, since it is irrelevant for the force or field generation through which conductor the current flows within a slot. Thus, the poor conductor utilization could be eliminated if the drive and bearing currents can be carried in a *combined winding*, i.e., the slot is fully utilized by one winding. Because of the vectorial (and not arithmetical) addition of the drive and bearing currents, which are 90° out of phase, this means that the rms current squared increases less than the winding resistance decreases when switching to a common conductor.

As explained earlier, in the 3 × 3 bearing winding, for example, axial connection of the star points enables a CM current component in the circumferential direction and thus a drive force, eliminating the ring-shaped drive winding. Such a combined 3 × 3 winding arrangement is shown in Fig. 6c. The operating principle of the combined 3 × 3 winding arrangement can also be understood as a ring-shaped drive winding, which is segmented into three parts in the circumferential direction, whereby now the three axially arranged three-phase winding systems can generate an additional radial bearing force by uneven distribution of the drive current in circumferential direction. This means that a CM current component in the circumferentially distributed windings is equivalent to ring currents and thus to a drive force, while the superimposed differential-mode (DM) components cause a radial redistribution of the drive current and thus a bearing force, but without changing the drive force. With this winding arrangement, the total currents in the individual phases are calculated as the sum of the drive and bearing currents as

$$i_{\{a,b,c\}\{A,B,C\}} = i_{\{A,B,C\}}^d + i_{\{a,b,c\}\{A,B,C\}}^b \quad (11)$$

Calculating the sum of the phase currents in rotary direction, only the drive current components remain again, i.e. $i_{\{a,b,c\}\{A,B,C\}} + i_{\{b,c,a\}\{A,B,C\}} + i_{\{c,a,b\}\{A,B,C\}} = 3 i_{\{A,B,C\}}^d$, which proves that the drive current component behaves like a CM component for the bearing current. On the other hand, summing the currents in the linear direction yields, as expected, a CM component of zero, i.e. $i_{\{a,b,c\}\{A,B,C\}} + i_{\{a,b,c\}\{B,C,A\}} + i_{\{a,b,c\}\{C,A,B\}} = 0$. As with the separated winding given in Fig. 6a, the combined 3 × 3 winding shown in Fig. 6c requires a total of 9 half-bridges and for the control only 6 currents have to be measured, however, the realization effort with 9 stator coils and the winding losses are significantly reduced.

For the sake of completeness, Fig. 6d alternatively shows the combined winding with a 2 × 3 bearing winding, where the circuit and measurement effort

increases again, so that the option in Fig. 6c is preferable.

5 Control Realization

At first glance, separated windings appear to be advantageous, at least with regard to control, since the respective drive and bearing currents can be controlled independently of each other. However, a combined winding does not mean that the control of the drive and bearing forces must also necessarily be combined; only the power electronics must also be combined, which however, as with the combined winding, advantageously leads to a reduction in power electronics complexity and semiconductor losses. Thus, if a separated drive and bearing control is used for the combined winding, only the commanded phase voltages $u_{\{A,B,C\}}^d$ for generating the drive currents and $u_{\{a,b,c\}\{A,B,C\}}^b$ for generating the bearing currents, must be added in advance before they are forwarded to the common power electronics, as it is shown in Fig. 7.

The control structures as well as the reference values for drive and z-position controller remain unchanged. For the drive current controller this means that according to (1) the d-component i_d^* is kept at zero, while the linear force generating q-component i_q^* is given by the outer z-position controller. The actual dq-currents i_d and i_q are calculated with the abc/dq-transform (cf. Fig. 2c) from the three actual CM current components i_A^d , i_B^d and i_C^d which are responsible for the driving force (cf. Fig. 7). Due to the axial star connection, i_C^d can also be determined from i_A^d and i_B^d . Vice versa, the dq-drive voltages $u_{\{d,q\}}^d$ are transformed into the phase drive voltages $u_{\{A,B,C\}}^d$ by means of Fig. 2b.

The xy-position controller is structured analogously, whereby according to (8) the q-components i_{xq}^* and i_{yq}^* are kept at zero, while the d-components i_{xd}^* and i_{yd}^* , which generate the bearing force, are defined by the two outer xy-position controllers (cf. Fig. 7). The actual dq-values are determined from all phase currents using the Park dq/abc-transform given in Fig. 5b. There, either only the DM components, as done in Fig. 7, or the total phase currents may be passed to the abc/dq-transform, because the abc/dq-transform removes all CM component anyway. Vice versa, the bearing voltages $u_{\{a,b,c\}\{A,B,C\}}^b$ are obtained from the dq-bearing voltages $u_{\{d,q\}\{A,B,C\}}^b$ by the dq/abc-transform in Fig. 5a.

Basically, this shows that with combined windings the control structure is equally simple or even simpler than with separated windings, because, for example, for the separated winding arrangement in Fig. 6b, another zero-component controller would have to be used. Therefore, for separated windings, the winding

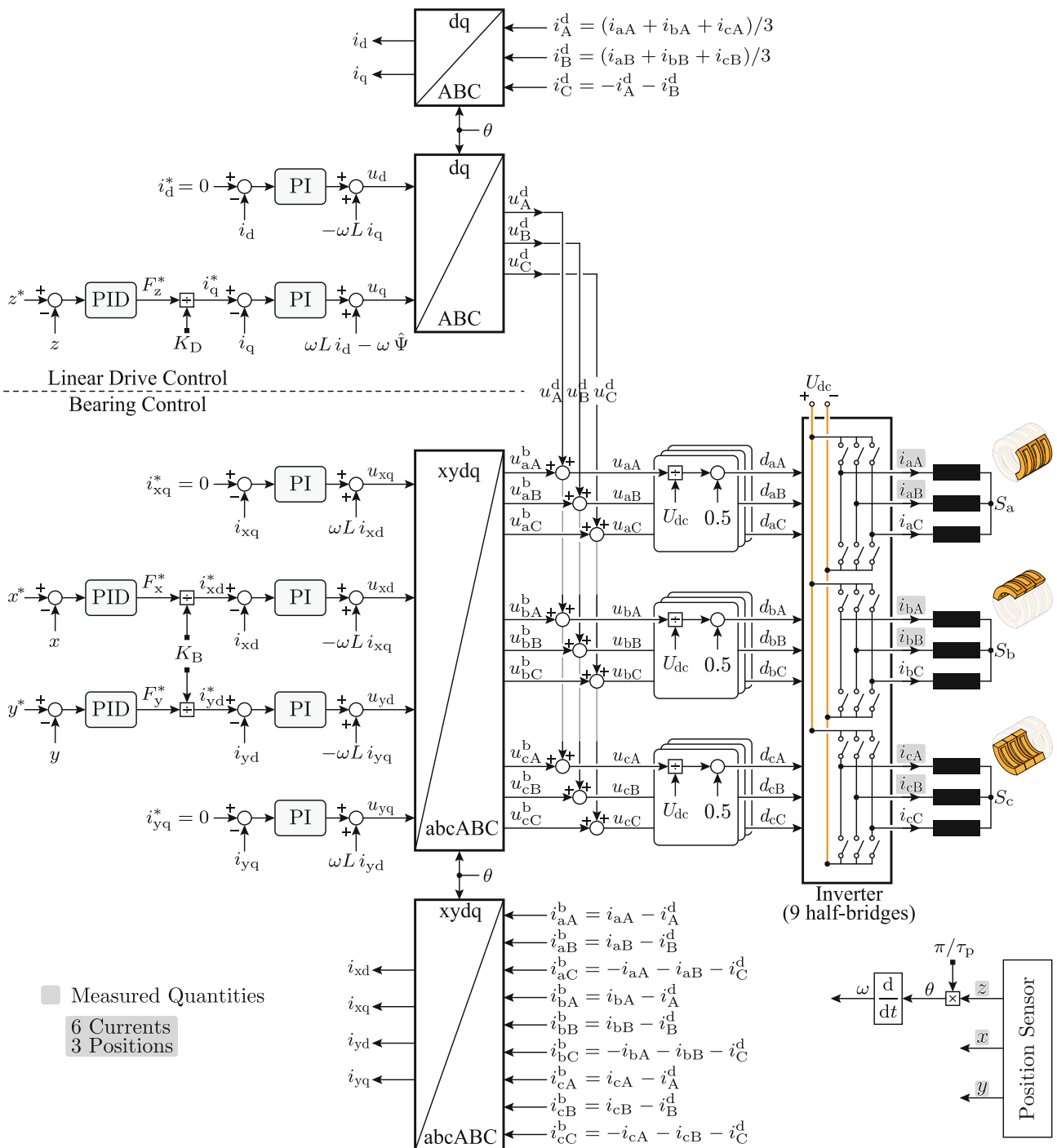


Fig. 7 Proposed control structure for the linear z- and the radial x-, y-position control of the MALTA employing a combined 3 × 3 winding arrangement

arrangement of Fig. 6a is preferred, the control structure of which is shown in the Appendix.

For sake of completeness, it must be mentioned that a combined control structure of the MALTA is also possible, cf. [19, 20].

6 Measurement Results

To verify the presented theoretical considerations, while using the control proposed in [19, 20], measurements are conducted on a MALTA hardware demonstrator (cf. Fig. 8a), which consists of two stator modules (Module 1 and Module 2). Each module features a combined 3 × 3 winding (cf. Fig. 6c) to control the radial xy-positions on both ends of

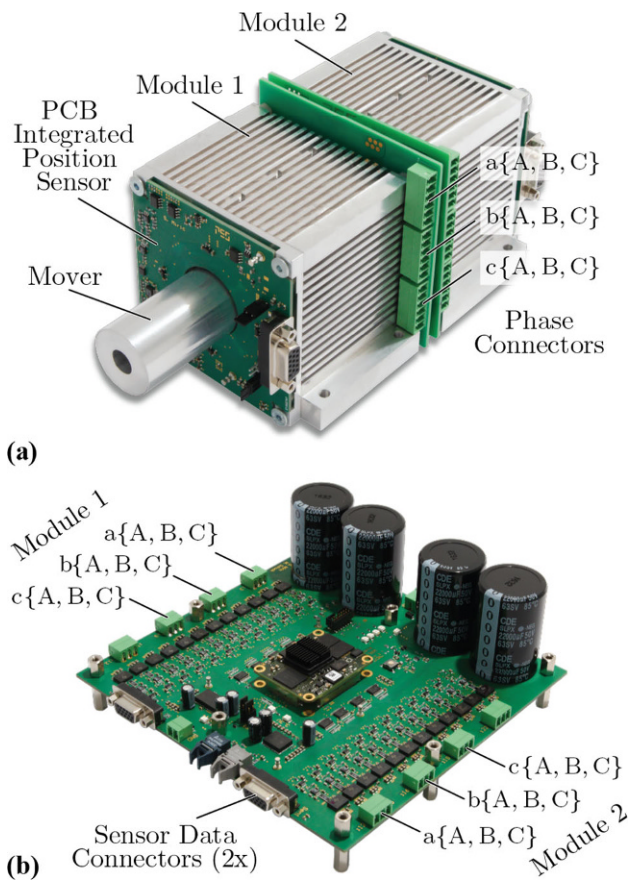


Fig. 8 Hardware prototypes: **a** MALTA realized with two modules, where each module contains a 3×3 combined winding. **b** Inverter with 18 half-bridges to supply the two modules of the MALTA

the long cylindrical mover, i.e. to eliminate tilting of the mover, and to drive together the mover in z -direction. Consequently, for the two modules in total 18 half-bridges are needed for the power electronics shown in Fig. 8b. The inverter drive is powered from a 45V DC-link voltage and switches at a frequency of 20kHz [20]. The eddy current sensors measuring the 4 radial positions of module 1 and module 2, i.e. x_1 , y_1 and x_2 , y_2 are PCB integrated (cf. Fig. 8a), while the linear position z is measured with surface-mounted Hall effect sensors.

The control system is discretized and implemented in C code on the processing platform Xilinx, Zynq Z-7020. The control system is executed at the switching frequency rate, i.e. 20kHz, which is limited by the available processing capability. In each control interrupt the current measurements of all 18 half-bridges are taken and transferred to the platform's memory simultaneously. The 18 individual pulse-width modulator are implemented in the fabric of the FPGA processing platform to drive the MALTA half-bridges.

The proper operation of the hardware prototypes is verified with a position step in z -direction, while the

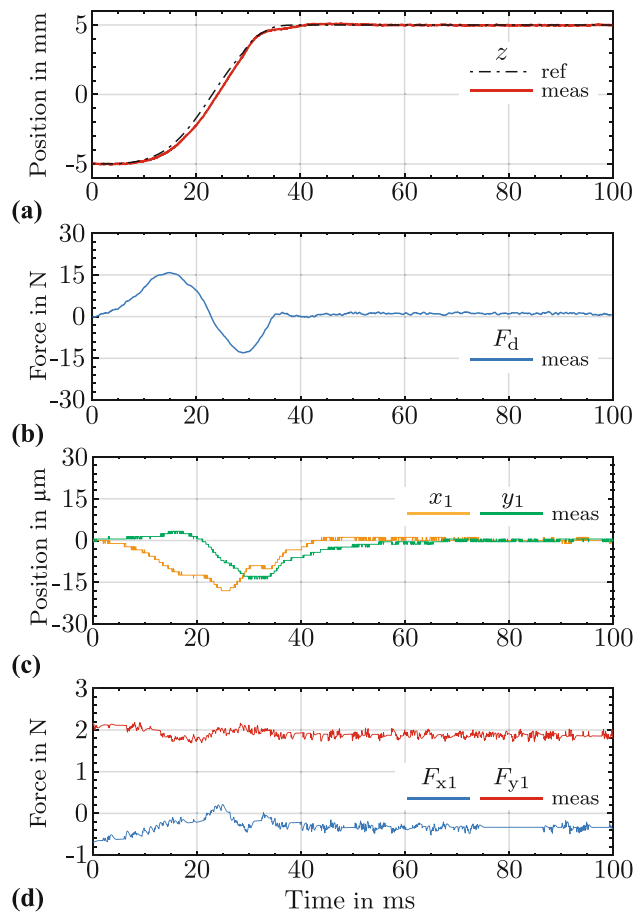


Fig. 9 Measurement results: **a** linear position step response z with a sigmoid 15 ms rise time reference; **b** linear drive force F_d ; **c** radial positions of module 1, x_1 , y_1 and **d** bearing force components of module 1, F_{x1} , F_{y1}

mover is kept by the bearing controllers in the center of the stator. The measurement results are depicted in Fig. 9, where the corresponding drive and bearing forces are shown in addition to the actual positions. It can be noted that during a linear step of 10 mm, the bearing controller keeps the mover within about 20 μm in radial direction. The offset of the radial force F_{y1} originates from the compensation of the weight of the mover.

7 Conclusions

In this paper, a novel magnetically levitated tubular linear actuator (MALTA) is described. To explain the drive and bearing force control, the generation of the drive force in the tubular linear actuator (TLA) with the ring-shaped windings is summarized first. Due to the circumferential symmetry, the TLA cannot generate any bearing forces. Therefore, novel winding realizations, a two-phase bearing winding with dedicated x - and y -coils for the direct control of the x - and y -force components and a three-phase bearing winding, are proposed. The operating principles of both windings are discussed and the impact of the linear

motion of the mover onto the bearing winding operation is explained. To achieve simultaneous drive and bearing force control, the drive and the bearing windings can be realized on the same stator (separated winding) or the bearing winding can carry the drive *and* the bearing current component (combined winding). The performance of each winding type is discussed in detail and it is concluded that the combined winding is advantageous over the separated one as it has better utilization of copper volume (higher force per unit of losses), facilitates dynamic allocation of the amount of copper used for the drive or for the bearing during operation, and easier stator manufacturing. Also, it is shown that the combined

winding does not have higher control effort, since the drive and the bearing current components can be split and fed independently to the drive and the bearing current controllers, which is shown in a detailed control diagram. As the MALTA winding has multiple three-phase systems, the importance of forming proper star connections is discussed, since, if not done properly, the winding arrangement could lead to parasitic drive forces or increased copper losses due to possibly occurring common-mode currents. Finally, measurement results verifying the proper operation of a MALTA prototype with combined windings are given.

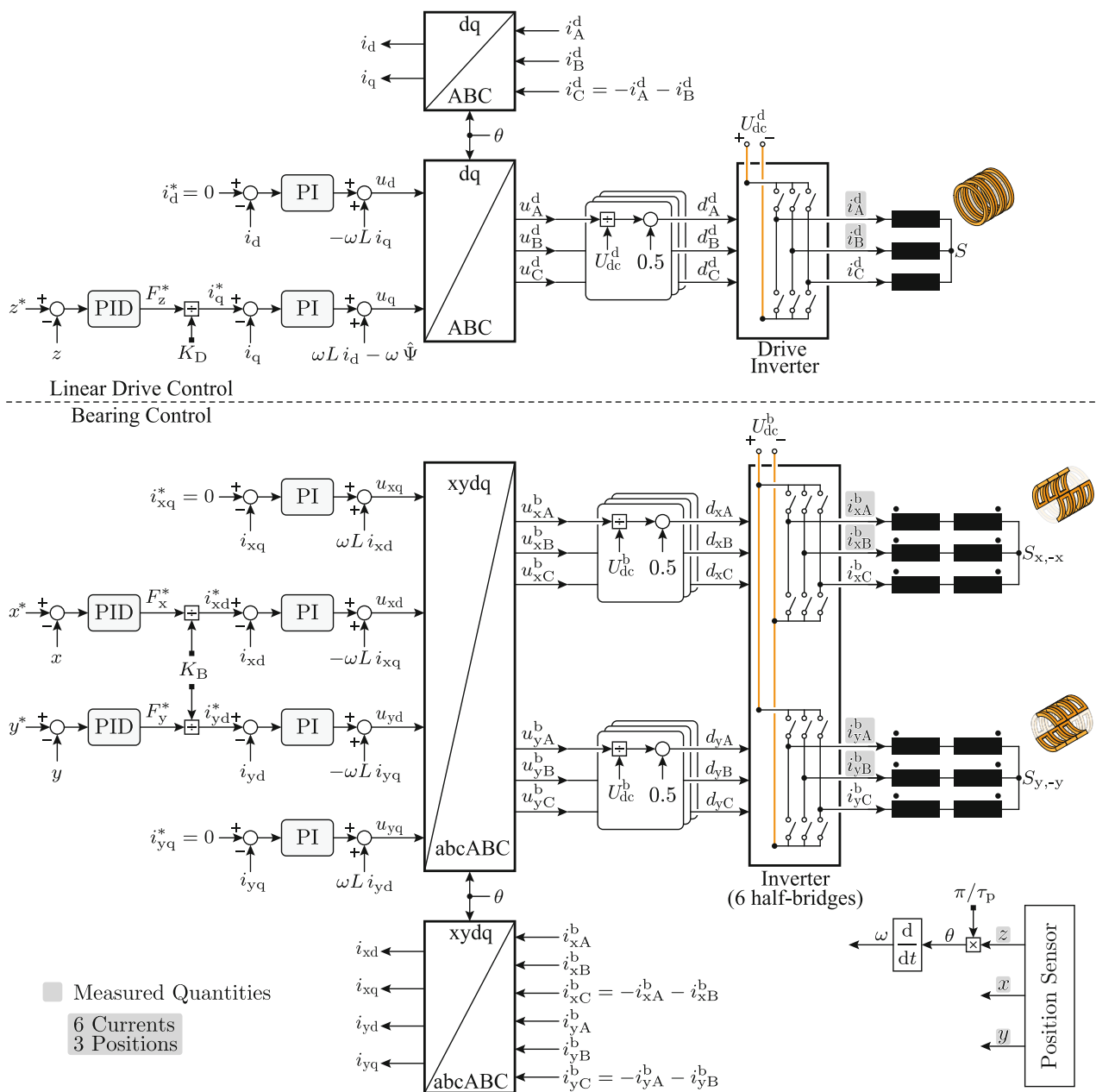


Fig. 10 Proposed control structure for the linear z- and the radial x-, y-position control of the MALTA employing separated 2 × 3 winding arrangements

Funding Open access funding provided by Swiss Federal Institute of Technology Zurich

Open Access This article is licensed under a Creative Commons Attribution 4.0 International License, which permits use, sharing, adaptation, distribution and reproduction in any medium or format, as long as you give appropriate credit to the original author(s) and the source, provide a link to the Creative Commons licence, and indicate if changes were made. The images or other third party material in this article are included in the article's Creative Commons licence, unless indicated otherwise in a credit line to the material. If material is not included in the article's Creative Commons licence and your intended use is not permitted by statutory regulation or exceeds the permitted use, you will need to obtain permission directly from the copyright holder. To view a copy of this licence, visit <http://creativecommons.org/licenses/by/4.0/>.

8 Appendix

In Fig. 10 the control structure for the *separated* 2×3 winding arrangement is depicted.

References

- Wang J, Howe D, Lin Z (2009) Design optimization of short-stroke single-phase tubular permanent-magnet motor for refrigeration applications. *IEEE Trans Ind Electron* 57(1):327–334
- Wang J, Howe D, Lin Z (2007) Comparative study of winding configurations of short-stroke, single phase tubular permanent magnet motor for refrigeration applications. In: *Proc. of the IEEE Industry Applications Annual Meeting*, pp 311–318
- Tsai NC, Chiang CW (2010) Design and analysis of magnetically-drive actuator applied for linear compressor. *Mechatronics* 20(5):596–603
- LG Inverter linear compressor. https://www.lg.com/levant_en/refrigerators/lg-gcb-244pn. Accessed 01.2022
- Wang J, Wang W, Atallah K, Howe D (2008) Comparative studies of linear permanent magnet motor topologies for active vehicle suspension. In: *Proc. of the IEEE Vehicle Power and Propulsion Conference*, pp 1–6
- Gysen BL, van der Sande TP, Paulides JJ, Lomonova EA (2011) Efficiency of a regenerative direct-drive electromagnetic active suspension. *IEEE Trans Veh Technol* 60(4):1384–1393
- Gysen BL, Paulides JJ, Janssen JL, Lomonova EA (2009) Active electromagnetic suspension system for improved vehicle dynamics. *IEEE Trans Veh Technol* 59(3):1156–1163
- Hodgins N, Keysan O, McDonald AS, Mueller MA (2011) Design and testing of a linear generator for wave-energy applications. *IEEE Trans Ind Electron* 59(5):2094–2103
- Kimoulakis NM, Kladas AG, Tegopoulos JA (2008) Power generation optimization from sea waves by using a permanent magnet linear generator drive. *IEEE Trans Magn* 44(6):1530–1533
- Prudell J, Stoddard M, Amon E, Brekken TK, Von Jouanne A (2010) A permanent-magnet tubular linear generator for ocean wave energy conversion. *IEEE Trans Ind Appl* 46(6):2392–2400
- Liu B, Bai J, Yin Z, Liu G, Liu Y, Zheng P (2021) Design and analysis of a novel primary-permanent-magnet transverse-flux linear generator for free-piston energy converter. In: *Proc. of the 24th IEEE International Conference on Electrical Machines and Systems (ICEMS)*, pp 1496–1499
- Chouder R, Stouffs P, Benabdesselam A (2021) A variant of the Fluidyne: the liquid piston ERICSSON engine. In: *Proc. of the E3S Web of Conferences*, vol 313, p 4001
- Cyusa CS, Payarou T, Barman D, Bertenyi T, Raphals P, Lai C, Pillay P (2021) Modeling and design of a tubular linear generator for direct-drive free-piston engine. In: *Proc. of the 47th Annual Conference of the IEEE Industrial Electronics Society (IECON)*, pp 1–6
- Overboom T, Jansen J, Lomonova E, Tacken F (2010) Design and optimization of a rotary actuator for a two-degree-of-freedom $z-\varphi$ module. *IEEE Trans Ind Appl* 46(6):2401–2409
- Meessen KJ, Paulides JJ, Lomonova EA (2010) Modeling and experimental verification of a tubular actuator for 20-g acceleration in a pick-and-place application. *IEEE Trans Ind Appl* 46(5):1891–1898
- Mirić S, Küttel P, Tüysüz A, Kolar JW (2018) Design and experimental analysis of a new magnetically levitated tubular linear actuator. *IEEE Trans Ind Electron* 66(6):4816–4825
- Mirić S, Tüysüz A, Kolar JW (2017) Comparative evaluation of linear-rotary actuator topologies for highly dynamic applications. In: *Proc. of the IEEE International Electric Machines and Drives Conference (IEMDC)*, pp 1–7
- Paulides JJ, Janssen JL, Lomonova EA (2009) Bearing lifetime of linear PM machines. In: *Proc. of the IEEE Energy Conversion Congress and Exposition*, pp 1083–1090
- Mirić SM, Giuffrida RV, Bortis D, Kolar JW (2019) Enhanced complex space vector modeling and control system design of multiphase magnetically levitated rotary-linear machines. *IEEE J Emerg Sel Topics Power Electron* 8(2):1833–1849
- Mirić S, Giuffrida R, Bortis D, Kolar JW (2020) Dynamic electromechanical model and position controller design of a new high-precision self-bearing linear actuator. *IEEE Trans Ind Electron* 68(1):744–755
- Zürcher F, Nussbaumer T, Kolar JW (2011) Motor torque and magnetic levitation force generation in bearingless brushless multipole motors. *IEEE/ASME Trans Mechatron* 17(6):1088–1097
- Mirić S (2021) Linear-rotary bearingless actuators (Ph.D. thesis, ETH Zurich)



Spasoje Mirić, (S'13) received B.Sc., M.Sc. and PhD degrees in electrical engineering from the University of Belgrade, School of Electrical Engineering in 2012, 2013 and 2018 respectively, with focus on power electronics systems and drives. In 2021 he defended his second PhD thesis at ETH Zurich at the Power Electronic Systems Laboratory (PES), in the advanced mechatronics systems area. More specifically, during his PhD project he focused on linear-rotary actuator systems with magnetic bearings, which resulted in two new machine topologies which have been patented. Since 2021, he is with PES as a post-doc researcher, focusing on WBG power converter optimization with hard and soft-switching, new modulation techniques of flying capacitor converters, wireless power transfer systems and eddy-current-based position sensor systems.



Johann Kolar, (M'89–F'10) received his M.Sc. and Ph.D. degree (summa cum laude) from the University of Technology Vienna, Austria, in 1997 and 1999, respectively. Since 1984, he has been working as an independent researcher and international consultant in close collaboration with the Vienna University of Technology, in the fields of power electronics, industrial electronics and high performance drive systems. He was appointed Assoc. Professor

and Head of the Power Electronic Systems Laboratory at the Swiss Federal Institute of Technology (ETH) Zurich on Feb. 1, 2001, and was promoted to the rank of Full Prof. in 2004. Dr. Kolar has proposed numerous novel converter concepts incl. the Vienna Rectifier, the Sparse Matrix Converter and the Swiss Rectifier, has spearheaded the development of x-million rpm motors, and has pioneered fully automated multi-objective power electronics design procedures. He has graduated 80+ Ph.D. students, has published 900+ journal and conference papers and 4 book chapters, and has filed 200+ patents. He has presented 30+ educational seminars at leading international conferences and has served as IEEE PELS Distinguished Lecturer from 2012–2016. He has received 40+ IEEE Transactions and Conference Prize Paper Awards, the 2014 IEEE Power Electronics Society R. David Middlebrook Achievement Award, the 2016 IEEE PEMC Council Award, the 2016 IEEE William E. Newell Power Electronics Award, the 2021 EPE Outstanding Achievement Award and 2 ETH Zurich Golden Owl Awards for excellence in teaching. He was elected to the U.S. National Academy of Engineering as an international member in 2021. The focus of his current research is on ultra-compact/efficient WBG converter systems, ANN-based design procedures, Solid-State Transformers, ultra-high speed drives, and bearingless motors.



Dominik Bortis, (SM'21) received the M.Sc. and Ph.D. degree in electrical engineering from the Swiss Federal Institute of Technology (ETH) Zurich, Switzerland, in 2005 and 2008, respectively. In May 2005, he joined the Power Electronic Systems Laboratory (PES), ETH Zurich, as a Ph.D. student. From 2008 to 2011, he has been a Postdoctoral Fellow and from 2011 to 2016 a Research Associate with PES. Since January 2016 Dr. Bortis is heading the research

group Advanced Mechatronic Systems at PES, which concentrates on ultra-high speed motors, bearingless drives, linear-rotary actuator and machine concepts with integrated power electronics. Targeted applications include e.g. highly dynamic positioning systems, medical systems, and future mobility concepts. Dr. Bortis has published 90+ scientific papers in international journals and conference proceedings. He has filed 30+ patents and has received 10 IEEE Conference Prize Paper Awards and 2 First Prize Transaction Paper Award.